trast to the leaky vasculature that is induced by overexpression of single vasculogenic growth factors such as VEGF (*32–34*), the HIF-induced vascular bed is stable (*31*). The more substantive neovascularization resulting from constitutive HIF-1α expression may reflect the fact that this transcription factor activates not only VEGF gene expression but also other genes important for the formation of new blood vessels [reviewed in (*35*)]. Selective inhibitors of the HPH enzymes may therefore merit investigation as new drugs for therapeutic angiogenesis.

References and Notes

1. G. L. Semenza, *Genes Dev.* **14**, 1983 (2000).
2. N. C. Bacon *et al.*, *Biochem. Biophys. Res. Commun.* **249**, 811 (1998).
3. J. R. Nambu, W. Chen, S. Hu, S. T. Crews, *Gene* **172**, 249 (1996).
4. H. Jiang, R. Guo, J. Powell-Coffman, *Proc. Natl. Acad. Sci. U.S.A.* **98**, 7916 (2001).
5. G. L. Wang, B. H. Jiang, E. A. Rue, G. L. Semenza, *Proc. Natl. Acad. Sci. U.S.A.* **92**, 5510 (1995).
6. L. E. Huang, J. Gu, M. Schau, H. F. Bunn, *Proc. Natl. Acad. Sci. U.S.A.* **95**, 7987 (1998).
7. P. J. Kallio, W. J. Wilson, S. O'Brien, Y. Makino, L. Poellinger, *J. Biol. Chem.* **274**, 6519 (1999).
8. S. Salceda, J. Caro, *J. Biol. Chem.* **272**, 22642 (1997).
9. M. E. Cockman *et al.*, *J. Biol. Chem.* **275**, 25733 (2000).
10. P. H. Maxwell *et al.*, *Nature* **399**, 271 (1999).
11. M. Ohh *et al.*, *Nature Cell Biol.* **2**, 423 (2000).
12. K. Tanimoto, Y. Makino, T. Pereira, L. Poellinger, *EMBO J.* **19**, 4298 (2000).
13. M. Ivan *et al.*, *Science* **292**, 464 (2001).
14. P. Jaakkola *et al.*, *Science* **292**, 468 (2001).
15. F. Yu, S. B. White, F. S. Lee, *Proc. Natl. Acad. Sci. U.S.A.* **98**, 9630 (2001).
16. G. L. Semenza, *Annu. Rev. Cell Dev. Biol.* **15**, 551 (1999).
17. K. I. Kivirikko, T. Pihlajaniemi, in *Advances in Enzymology and Related Areas of Molecular Biology*, D. L. Purich, Ed. (Wiley, New York, 1998), vol. 72, pp. 325–398.
18. Coding regions were amplified by reverse transcriptase polymerase chain reaction (RT-PCR) from total RNA prepared from human cell lines with oligonucleotides derived from the following sequences (GenBank accession number): HPH-1 (XM_012332), HPH-2 (AF229245), HPH-3 (BC001723), candidate A (NM_017732), candidate B (AK022130), candidate C (AK001580), and candidate D (AK023553). A splice variant of HPH-2 was used in which residues 76 to 177 were omitted. Point mutations in HPH-1 were generated by PCR. Each cDNA was cloned into the pcDNA3.1/V5-HIS vector (Invitrogen) in frame with the COOH-terminal V5-HIS tag.
19. Candidate polypeptides were synthesized with the TNT Coupled Reticulocyte Lysate System (Promega) for 1 hour at 30°C. Expression of each gene product was confirmed by Western blot analysis with an antibody specific for the COOH-terminal V5 tag. 12.5 μl of each in vitro transcription/translation reaction was incubated for 30 min at 30°C in a reaction buffer containing 20 mM tris-Cl (pH 7.5), 5 mM KCl, 1.5 mM MgCl$_2$, 1 mM dithiothreitol, 2 mM 2-oxoglutarate, 2 mM ascorbate, and 250 μM FeSO$_4$ in the presence of 30 μl of ImmunoPure Immobilized Streptavidin beads that had previously been incubated with 1 μg of peptide for 30 min at room temperature and washed three times to remove excess peptide. After incubation, the beads were washed three times with 1 ml of cold NTEN buffer [20 mM tris-Cl (pH 8.0), 100 mM NaCl, 1 mM EDTA, and 0.5% NP-40] and incubated for 10 min at 4°C with about 35 kcpm of [^{35}S]-labeled human VHL in 500 μl of EBC buffer [50 mM tris-Cl (pH 8.0), 120 mM NaCl, and 0.5% NP-40]. The beads were washed three times with cold NTEN buffer, and bound [^{35}S]-VHL

was measured by scintillation counting. [^{35}S]-labeled human VHL was synthesized from the human VHL cDNA cloned into the pcDNA3.1/V5-HIS vector (Invitrogen) with the TNT Coupled Reticulocyte Lysate System (Promega) and [^{35}S]-L-Met (Amersham Pharmacia Biotech) and desalted with a PD-10 column (Amersham Pharmacia Biotech).
20. Single-letter abbreviations for the amino acid residues are as follows: A, Ala; C, Cys; D, Asp; E, Glu; F, Phe; G, Gly; H, His; I, Ile; K, Lys; L, Leu; M, Met; N, Asn; P, Pro; Q, Gln; R, Arg; S, Ser; T, Thr; V, Val; W, Trp; and Y, Tyr.
21. HPH-2 was cloned into the pMBP-parallel1 vector (*36*) and expressed in the BL21-CodonPlus-RIL *E. coli* strain (Stratagene). Recombinant protein was purified by virtue of the NH$_2$-terminal MBP protein with amylose resin (New England Biolabs) and eluted in the presence of 10 mM maltose.
22. One microgram of peptide was incubated with 1 μg of recombinant HPH-2 in reaction buffer for 1 hour at 30°C. Peptide mass was determined by matrix-assisted laser desorption/ionization–time-of-flight mass spectrometry.
23. Transfection experiments were performed as in (*24*) with DNA amounts indicated in the text. Western blot analysis with an antibody specific for the COOH-terminal V5 tag was used to confirm expression of each polypeptide after transfection of 1 μg of each expression vector.
24. R. K. Bruick, *Proc. Natl. Acad. Sci. U.S.A.* **97**, 9082 (2000).
25. B. Adryan, H.-J. Decker, T. S. Papas, T. Hsu, *Oncogene* **19**, 2803 (2000).
26. E. Ma, G. G. Haddad, *Mol. Brain Res.* **73**, 11 (1999).
27. KC167 cells were maintained at 24°C in CCM 3 media (HyClone). Cells were treated as follows: initially, 4 × 10^5 KC167 cells were incubated for 7 days in the presence of 25 μg of double-stranded RNAs of about 700 base pairs in length generated with the T7

MEGAscript Kit (Ambion) with double-stranded RNA refreshed daily. Cells were incubated under normoxic (20% O$_2$) or hypoxic (1% O$_2$, 99% N$_2$) conditions for an additional 15 hours, and total RNA was prepared with RNA STAT-60 (Tel-Test). RNAs were resolved by electrophoresis in a 1.2% agarose gel in the presence of 1.8% formaldehyde, transferred to nitrocellulose filters, and hybridized with the indicated ^{32}P-labeled DNA probes.
28. N. V. Iyer *et al.*, *Genes Dev.* **12**, 149 (1998).
29. H. E. Ryan, J. Lo, R. S. Johnson, *EMBO J.* **17**, 3005 (1998).
30. E. A. Lipscomb, P. D. Sarmiere, R. S. Freeman, *J. Biol. Chem.* **276**, 5085 (2001).
31. D. A. Elson *et al.*, *Genes Dev.* **15**, 2520 (2001).
32. M. Detmar *et al.*, *J. Invest. Dermatol.* **111**, 1 (1998).
33. F. Larcher, R. Murillas, M. Bolontrade, C. J. Conti, J. L. Jorcano, *Oncogene* **17**, 303 (1998).
34. G. Thurston *et al.*, *Science* **286**, 2511 (1999).
35. R. K. Bruick, S. L. McKnight, *Genes Dev.* **15**, 2497 (2001).
36. P. Sheffield, S. Garrard, Z. Derewenda, *Prot. Express. Pur.* **15**, 34 (1999).
37. We thank members of the McKnight, Abrams, and Wang laboratories for advice and encouragement; L. Wu, C. Michnoff, and F. Hirani for technical assistance; L. Huang for peptide synthesis; Y. Zhao for assistance with mass spectrometry; and N. Grishin for assistance with database searches. Funded by a National Research Service Award from the NIH (R.K.B.), NIH grants DK52031 and MH59388 (S.L.M.), and endowment funds provided to S.L.M. by an anonymous donor.

Reconstitution of Physiological Microtubule Dynamics Using Purified Components

Kazuhisa Kinoshita,[1]* Isabelle Arnal,[1,2]† Arshad Desai,[1] David N. Drechsel,[1] Anthony A. Hyman[1]*

Microtubules are dynamically unstable polymers that interconvert stochastically between polymerization and depolymerization. Compared with microtubules assembled from purified tubulin, microtubules in a physiological environment polymerize faster and transit more frequently between polymerization and depolymerization. These dynamic properties are essential for the functions of the microtubule cytoskeleton during diverse cellular processes. Here, we have reconstituted the essential features of physiological microtubule dynamics by mixing three purified components: tubulin; a microtubule-stabilizing protein, XMAP215; and a microtubule-destabilizing kinesin, XKCM1. This represents an essential first step in the reconstitution of complex microtubule dynamics–dependent processes, such as chromosome segregation, from purified components.

Microtubules polymerize and depolymerize by the addition and loss of αβ-tubulin dimer subunits from their ends (*1*). Polymerizing and depolymerizing microtubules coexist and infrequently interconvert between these two states, a behavior known as dynamic instability (*2*). The transition of a polymerizing microtubule to a depolymerizing state is referred to as a catastrophe, and the converse transition is referred to as a rescue (*3*). Mi-

crotubules exhibit dynamic instability when assembled from purified tubulin (*3, 4*) and in a physiological cytoplasmic environment (*5–10*), but there are notable differences between the two. In a physiological environment, microtubules polymerize about fourfold faster than a similar concentration of purified tubulin. At the polymerization rates observed in physiological conditions, purified tubulin has a near-zero rate of catastrophe. In contrast,

microtubules in cells and in cytoplasmic extracts have a high catastrophe rate despite their high polymerization rate.

Clues to the dynamic behavior of microtubules in physiological conditions have come from the identification of proteins that modulate microtubule dynamics. Microtubule-associated proteins (MAPs) increase the polymerization rate of microtubules, whereas destabilizing proteins increase the rate of catastrophe. In *Xenopus* egg extracts, the dominant stabilizing MAP appears to be XMAP215, a member of an evolutionary conserved protein family (*11*, *12*). Depleting XMAP215 prevents microtubule growth, whereas depletion of other MAPs has so far had little effect (*12*, *13*). The dominant catastrophe factor in *Xenopus* extracts is XKCM1 (*14*, *15*), a member of the KinI subfamily of kinesins (*16*). Depletion of XKCM1 markedly stabilizes microtubules, whereas depletion of other catastrophe factors have to date had more modest effects (*14*, *17*).

Depletion experiments suggest that these two factors oppose each other to determine the stability of the microtubule lattice in *Xenopus* extracts. Depletion of XMAP215 destabilizes microtubules, and subsequent inhibition of XKCM1 causes the microtubules in XMAP215-depleted extracts to become stable again (*12*). These results suggest that the coordinate action of only these two proteins on tubulin may explain why microtubules in cells can both polymerize rapidly and exhibit high catastrophe rates. We tested

[1]Max Planck Institute of Molecular Cell Biology and Genetics, Pfotenhauerstrasse 108, 01307, Dresden, Germany. [2]European Molecular Biology Laboratory, Meyerhofstrasse 1, 69117 Heidelberg, Germany.

*To whom correspondence should be addressed. E-mail: kinoshita@mpi-cbg.de, hyman@mpi-cbg.de
†Present address: Equipe ATIPE, UMR 6026, Université de Rennes 1, Campus de Beaulieu, Bt 13, 35042 Rennes Cedex, France.

this hypothesis by combining these two factors with purified tubulin in vitro and examining the behavior of microtubules. We first produced full-length recombinant His$_6$-tagged XMAP215 and XKCM1 (*18*). As expected, XKCM1 reduced microtubule length whereas XMAP215 increased microtubule length (Fig. 1) (*15*, *18–20*). However, when added together, XMAP215 opposed the ability of XKCM1 to decrease the average length of microtubules (Fig. 1) (*18*). Therefore, we conclude that the relative activities of XMAP215 and XKCM1 can determine the steady-state length of microtubules assembled from purified tubulin in the absence of other factors.

In *Xenopus* extracts, XMAP215 suppresses the ability of XKCM1 to induce microtubule catastrophe (*12*). To test if this suppression can be observed with purified proteins, we set up a real-time assay in which the behavior of individual microtubules was monitored by video-enhanced differential interference contrast (VE-DIC) microscopy (*21*). Briefly, purified centrosomes were adsorbed to the surface of a perfusion chamber, and tubulin was perfused into the chamber and allowed to polymerize (*18*). Different combinations of factors with tubulin were then perfused into the chamber, and the number of microtubules transiting from polymerization to depolymerization after perfusion was quantified (*18*). After perfusion of 150 nM XKCM1 together with tubulin, 60 to 70% of the microtubules transited to depolymerization (Fig. 2). Adding XMAP215 together with 150 nM XKCM1 and tubulin suppressed the number of microtubules transiting to depolymerization in an XMAP215 concentration–dependent manner (Fig. 2). This result with three purified components leads us to conclude that the suppression of XKCM1-induced catastrophes by XMAP215 in cyto-

plasmic extracts is a direct consequence of the action of these two proteins at microtubule ends.

The above results suggested that potentially a steady-state mixture of tubulin, XMAP215, and XKCM1 could reconstitute the two characteristic physiological features of dynamic instability: rapid polymerization and high catastrophe rates (Table 1). To explore this idea, we developed conditions in which the dynamic behavior of these microtubules could be directly observed by DIC microscopy (*22*). The concentrations of these proteins in *Xenopus* extracts have been estimated to be 25 μM (tubulin) (*23*), 60 nM (XKCM1) (*14*), and 0.6 μM (XMAP215) (*12*). Using a mixture of 25 μM tubulin, 0.2 μM XKCM1, and 0.8 μM XMAP215, we were able to reconstitute physiological parameters of dynamic instability (*18*). A typi-

A Before perfusion (Tubulin alone) / After perfusion

Perfusion with
i) Control buffer
ii) XKCM1
iii) XKCM1 + XMAP215

Fig. 2. XMAP215 inhibits catastrophes induced by XKCM1. (**A**) Images of microtubules before and 4 min after perfusion (*21*). Microtubules were polymerized from centrosomes with 33 μM tubulin (left). Perfusion chambers were perfused with tubulin (33 μM) and control buffer (i), 0.15 μM XKCM1 (ii), or 0.15 μM XKCM1 + 1.2 μM XMAP215 (iii). Bar, 10 μm. (**B**) The percentage of shrinking microtubules after perfusion of XKCM1 (0.15 μM) + XMAP215 (0, 0.6, or 1.2 μM) was plotted versus the concentration of XMAP215.

Fig. 1. XMAP215 opposes XKCM1 in the regulation of microtubule length in vitro. (**A** and **B**) XKCM1 (62.5 nM, +XKCM1) or control buffer (−XKCM1) was mixed with 15 μM tubulin and centrosomes in the absence (A) or presence (B) of 125 nM XMAP215. Microtubule asters are shown after 5 min of incubation at 37°C (*20*). Bars, 25 μm. (**C**) Quantification of microtubule length in (A) (−XMAP; open columns) and (B) (+XMAP; solid columns). Arrowheads indicate the average length of microtubules (−XMAP, open arrowheads; + XMAP, solid arrowheads).
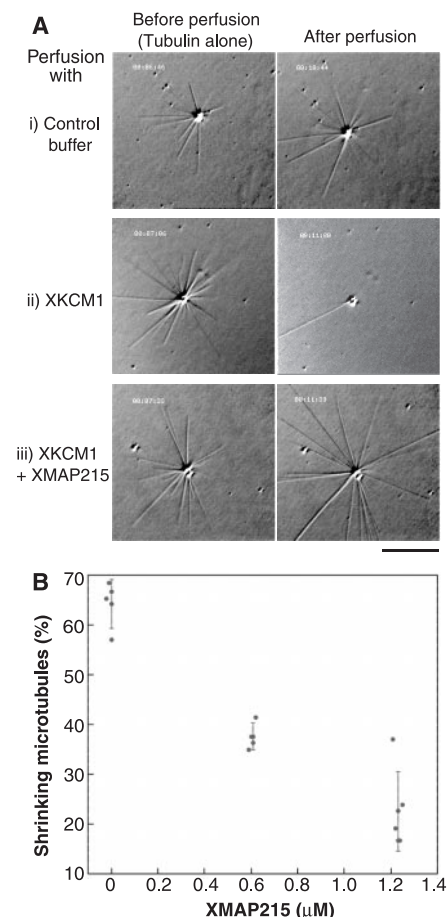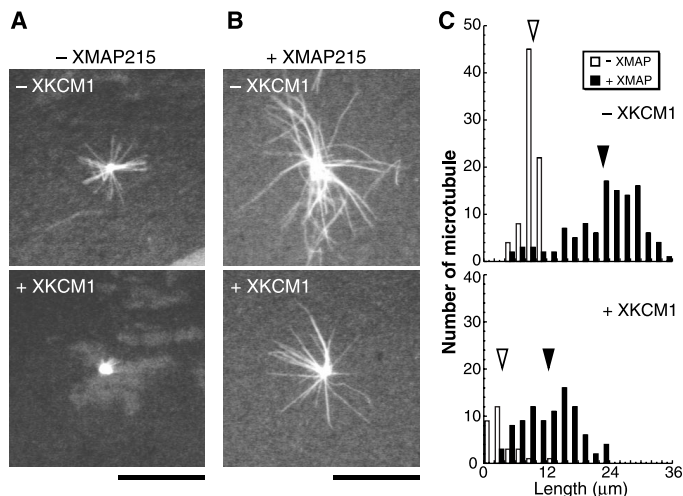
Table 1. Comparison of the parameters of microtubule dynamics in vitro and in vivo. Dashes indicate that no microtubules were formed. NA, not applicable.

| Parameter | In vitro (25 μM tubulin) | | | | In vivo | | | | |
| | Tubulin alone | +0.8 μM XMAP215 | + 0.2 μM XKCM1 | + 0.8 μM XMAP215 + 0.2 μM XKCM1 | Xenopus egg extracts | | Newt lung cells‡ | Mammalian LLCPK-1 cells§ | |
					Interphase*	Mitotic†		Interphase	Mitotic
Growth (V_g) (μm/min)	2.56 (±0.75)	6.76 (±1.76)	−	8.73 (±3.72)	7.10	11.40	7.20	11.50	12.80
Shrinkage (V_s) (μm/min)	NA	NA	−	19.94 (±5.20)	9.40	13.50	17.30	13.10	14.10
Catastrophe (F_{cat}) (events/min)	0.04	0	−	1.06	0.69	2.44	0.84	1.56	3.48
Rescue (F_{res}) (events/min)	NA	NA	−	1.30	1.08	0.70	2.64	10.50	2.70

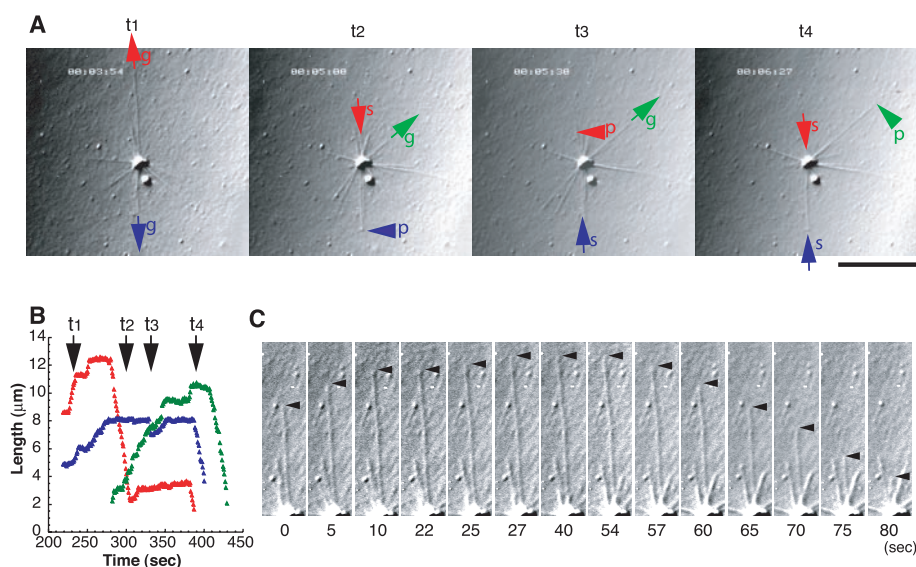*Verde et al. (9). †Tournebize et al. (10). ‡Cassimeris et al. (5). §Rusan et al. (7).

Fig. 3. Reconstitution of physiological microtubule dynamics with XMAP215 and XKCM1. (**A**) Dynamic instability behavior of microtubules in the presence of 25 μM tubulin, 0.8 μM XMAP215, and 0.2 μM XKCM1 at 30°C (22). VE-DIC images of microtubules are shown at various time points (t_1 to t_4). g, growing microtubule; p, pausing microtubule; s, shrinking microtubule. The colors of arrows and arrowheads in (A) correspond to the traces of microtubules in (B). (**B**) Life-history traces of the microtubules. (**C**) Fate of a single microtubule. Scale bars, 10 μm.

crotubule length in vivo (31). Thus, this three-component system may represent a conserved module that generates the characteristic behavior of physiological microtubules. The simple mixture we describe here will serve as a starting point for analyzing the effect of other microtubule regulators, such as XMAP230 and Op18 (13, 17), in a reconstruction-type approach. Furthermore, it represents an important step in the pursuit of the eventual reconstitution of complex dynamic microtubule assemblies, such as the mitotic spindle, from purified components.

References and Notes
1. A. Desai, T. J. Mitchison, *Annu. Rev. Cell Dev. Biol.* **13**, 83 (1997).
2. T. Mitchison, M. Kirschner, *Nature* **312**, 237 (1984).
3. R. A. Walker et al., *J. Cell Biol.* **107**, 1437 (1988).
4. T. Horio, H. Hotani, *Nature* **321**, 605 (1986).
5. L. Cassimeris, N. K. Pryer, E. D. Salmon, *J. Cell Biol.* **107**, 2223 (1988).
6. J. H. Hayden, S. S. Bowser, C. L. Rieder, *J. Cell Biol.* **111**, 1039 (1990).
7. N. M. Rusan, C. J. Fagerstrom, A. M. Yvon, P. Wadsworth, *Mol. Biol. Cell* **12**, 971 (2001).
8. L. D. Belmont, A. A. Hyman, K. E. Sawin, T. J. Mitchison, *Cell* **62**, 579 (1990).
9. F. Verde, M. Dogterom, E. Stelzer, E. Karsenti, S. Leibler, *J. Cell Biol.* **118**, 1097 (1992).
10. R. Tournebize et al., *EMBO J.* **16**, 5537 (1997).
11. D. L. Gard, M. W. Kirschner, *J. Cell Biol.* **105**, 2203 (1987).
12. R. Tournebize et al., *Nature Cell Biol.* **2**, 13 (2000).
13. B. Cha, L. Cassimeris, D. L. Gard, *J. Cell Sci.* **112**, 4337 (1999).
14. C. E. Walczak, T. J. Mitchison, A. Desai, *Cell* **84**, 37 (1996).
15. A. Desai, S. Verma, T. J. Mitchison, C. E. Walczak, *Cell* **96**, 69 (1999).
16. A. W. Hunter, L. Wordeman, *J. Cell Sci.* **113**, 4379 (2000).
17. L. D. Belmont, T. J. Mitchison, *Cell* **84**, 623 (1996).
18. Supplementary Web material is available on *Science* Online at www.sciencemag.org/cgi/content/full/294/5545/1340/DC1.
19. R. J. Vasquez, D. L. Gard, L. Cassimeris, *J. Cell Biol.* **127**, 985 (1994).
20. For fixed time point assay, purified proteins or control buffer was mixed with 1.5 μM rhodamine-labeled and 13.5 μM unlabeled tubulin together with centrosomes in BRB80 [80 mM K-Pipes, 1 mM MgCl₂, 1 mM EGTA (pH 6.8)] in the presence of 1 mM guanosine 5′-triphosphate (GTP), 1.5 mM adenosine

cal aster growing under these conditions is shown in Fig. 3. Quantification of microtubule dynamics revealed that this simple three-component mixture recapitulated the essential features of physiological microtubule dynamic instability (Table 1).

Why does the three-component mixture reconstitute physiological dynamic instability? XMAP215 alone accounts for the observed fast polymerization rate, whereas XKCM1 alone prevents any assembly of microtubules, presumably as a consequence of inducing a catastrophe rate that is too high (Table 1) (18). In the three-component mixture, XMAP215 must partially suppress the catastrophe-promoting activity of XKCM1 in order to generate the combination of fast

polymerization and high catastrophe rates. This partial suppression of XKCM1-induced catastrophes by XMAP215 (Fig. 2) without influencing the polymerization rate (Table 1) is central to understanding why the three-component mixture reconstitutes the combination of fast polymerization and high catastrophe rates.

Taken together with the results in *Xenopus* extracts (12, 14), we believe that the essential features of dynamic instability in *Xenopus* egg extracts are derived from the sole action of these two factors on tubulin. These factors are conserved from yeast through mammals (24–31), and at least in *Saccharomyces cerevisiae*, orthologous factors oppose each other in the control of mi-

5′-triphosphate (ATP), 100 mM KCl, and 1 mM di-thiothreitol (DTT). Samples were incubated at 37°C for 5 min, fixed with 0.5% glutaraldehyde, and squashed under cover slips.

21. An Olympus VE-DIC equipped with Plan Apo 60×/1.4 numerical aperture DIC lens and Hamamatsu 2400 newvicon video camera was used. Images were enhanced with an Argus 20 (Hamamatsu). Centrosomes were first perfused into perfusion chamber on ice. Perfusion chamber surfaces were blocked by incubation with 5 mg/ml casein in BRB80 and washed with 0.5% NP-40 in BRB80. Microtubule assembly was initiated by perfusion of 33 μM tubulin in BRB80 containing 1 mM GTP, 1.5 mM ATP, 100 mM KCl, 1 mM DTT, and 0.5 mg/ml casein. Subsequently, tubulin with purified proteins or control buffer was perfused, and the fate of microtubules was monitored.
22. Modified from the perfusion assay described in (21). After absorption of centrosomes, blocking with casein, and washing with NP-40, 25 μM tubulin with purified proteins or control buffer in BRB80 containing 1 mM GTP, 1.5 mM ATP, 60 mM KCl, 1 mM DTT, 0.5% NP-40, and 0.5 mg/ml casein were perfused into the chamber on ice. The perfusion chamber was warmed to 30°C and sealed. Recording was performed at 30°C every 1 s for 10 min. Analysis of microtubule dynamics was done as described (10). Catastrophe frequency was calculated by dividing the total number of events by the duration of growth and pause phases.
23. D. L. Gard, M. W. Kirschner, J. Cell Biol. 105, 2191 (1987).
24. K. Nabeshima et al., Genes Dev. 9, 1572 (1995).
25. P. J. Wang, T. C. Huffaker, J. Cell Biol. 139, 1271 (1997).
26. S. Charrasse et al., J. Cell Sci. 111, 1371 (1998).
27. L. R. Matthews, P. Carter, M. D. Thierry, K. Kemphues, J. Cell Biol. 141, 1159 (1998).
28. C. F. Cullen, P. Deak, D. M. Glover, H. Ohkura, J. Cell Biol. 146, 1005 (1999).
29. R. Graf, C. Daunderer, M. Schliwa, J. Cell Sci. 113, 1747 (2000).
30. L. Wordeman, T. J. Mitchison, J. Cell Biol. 128, 95 (1995).
31. F. Severin, B. Habermann, T. Huffaker, T. Hyman, J. Cell Biol. 153, 435 (2001).
32. We are grateful to C. E. Walczak for the cDNA clone of XKCM1; S. Berthold and F. Senger for help with protein purification; E. Karsenti and his group for helpful discussion; and H. Funabiki, J. Howard, K. Oegema, E. Tanaka, and W. Zachariae for comments on the manuscript. Supported by a Human Frontier Science Program Organization long-term fellowship and a grant from the Deutsche Forschungsgemeinschaft (K.K.), a Max-Planck-Gesellschaft fellowship and a grant from the Fondation pour la Recherche Médicale (I.A.), and fellowships from the European Molecular Biology Organization and the American Cancer Society (A.D.).

A Phosphatase Associated with Metastasis of Colorectal Cancer

Saurabh Saha, Alberto Bardelli,* Phillip Buckhaults, Victor E. Velculescu, Carlo Rago, Brad St. Croix, Katharine E. Romans, Michael A. Choti, Christoph Lengauer, Kenneth W. Kinzler,† Bert Vogelstein†

To gain insights into the molecular basis for metastasis, we compared the global gene expression profile of metastatic colorectal cancer with that of primary cancers, benign colorectal tumors, and normal colorectal epithelium. Among the genes identified, the PRL-3 protein tyrosine phosphatase gene was of particular interest. It was expressed at high levels in each of 18 cancer metastases studied but at lower levels in nonmetastatic tumors and normal colorectal epithelium. In 3 of 12 metastases examined, multiple copies of the PRL-3 gene were found within a small amplicon located at chromosome 8q24.3. These data suggest that the PRL-3 gene is important for colorectal cancer metastasis and provide a new therapeutic target for these intractable lesions.
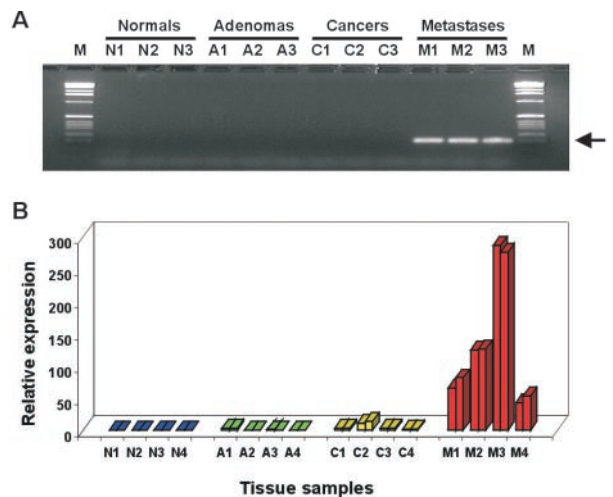
Metastasis is the neoplastic process responsible for most deaths from cancer because the primary tumors can usually be surgically removed. Metastatic cells undergo cytoskeletal changes, loss of adhesion, and enhanced motility and express proteolytic enzymes that degrade the basement membrane (1–3). However, much remains to be learned about this lethal process, and further progress is contingent upon identifying novel genes and pathways that are consistently and specifically altered in metastatic lesions.

In the case of colorectal tumorigenesis, the genes associated with initiation and progression to the invasive (cancerous) stage are well known (4). However, no gene has been shown to be consistently and specifically activated in liver metastases, the lesions that are usually responsible for the deaths of colorectal cancer patients. To learn which genes might be involved in this process, we performed global gene expression profiles of liver metastases using serial analysis of gene expression (SAGE) technology (5). We first prepared a SAGE library from microdissected metastases (6). Surprisingly, we found that many of the transcripts identified in these libraries were characteristic of normal hepatic or inflammatory cells, precluding quantitative analysis (7). To produce a more specific profile of metastatic epithelial cells, we developed an immunoaffinity fractionation procedure to purify colorectal epithelial cells from contaminating stromal and hepatic cells (8). A SAGE library was prepared from cells purified in this manner, yielding ~95,000 tags representing at least 17,324 transcripts (6). These tags were compared with ~4 million tags derived from diverse SAGE libraries, particularly those from normal and malignant (but nonmetastatic) colorectal epithelium (9). One hundred and forty-four transcripts were represented at significantly higher levels in the metastasis library than in the other libraries, while 79 transcripts were

Howard Hughes Medical Institute, The Oncology Center, Department of Surgery, and Program in Cellular and Molecular Medicine, Johns Hopkins Medical Institutions, Baltimore, MD 21231, USA.

*On leave from the University of Torino, Institute for Cancer Research, 10060 Candiolo, Torino, Italy.
†To whom correspondence should be addressed. E-mail: kinzlke@jhmi.edu (K.W.K.); vogelbe@welch.jhu.edu (B.V.)

Fig. 1. PRL-3 expression in human colorectal tumors of different stage. The expression of PRL-3 was evaluated by real-time PCR (8) and compared with that of the β-amyloid precursor protein (APP) gene, shown previously to be expressed at nearly identical levels in normal and neoplastic colorectal tissues (9). The metastases analyzed in this experiment were derived from patients other than the ones from whom the normal epithelium and other lesions were derived. Epithelial cells were purified as described (8). (**A**) Gel of RT-PCR products from normal colorectal epithelium (N1 to N3), adenomas (A1 to A3), primary cancers (C1 to C3), and metastases (M1 to M3). Real-time PCR was performed for 24 cycles, when RT-PCR products from the metastases were evident but before signals from the other lesions had appeared. Arrow indicates the PRL-3 RT-PCR product of 198 bp. Lane M, molecular size markers. (**B**) Results are expressed as the ratio between PRL-3 and APP expression and are normalized to the average expression in adenomas. Duplicates are shown for each analysis.